

Quantifying Spatial Variability in Forest Plots

Gavin Corral

USDA NASS, 1400 Independence Ave, Washington DC

Abstract

Researchers have begun to realize that treating individual trees within a single plot as independent is erroneous (Penttinen et al. 1992, Mateu et al. 1998). Our goal was to reproduce the induced spatial dependence of plot data and to assess the efficacy of redundancy analysis for testing spatial variability. We designed a range of conditions for plots that included manipulation of microsite productivity and spatial pattern complexity. Simulated populations without confounding effects of competition and mortality were analyzed using redundancy analysis (RDA) to quantify spatial variability and partial redundancy analysis (pRDA) to test for spatial dependence. We found that increased variation in growth and decreased average tree size differences among microsites resulted in decreased efficacy of variation partitioning by RDA and decreased efficacy of spatial dependence testing by pRDA. However, spatial pattern complexity of the simulated plots caused mixed results of variation partitioning. The results indicated that RDA and pRDA are reliable methods of analysis and are suitable for applications to field data.

Key Words: Forestry, Redundancy Analysis, Simulation, Spatial Analysis.

1. Introduction

In order to investigate spatial effects on tree growth, we developed a method to simulate forest plots, then tested the efficacy of statistical methods to detect and quantify spatial variability in forest plots. A lack of information exists on dependable methods to detect, quantify, and map spatial heterogeneity in small-scale forest plots (Marignani et al. 2007, Hou et al. 2015). An increased effort to improve plot uniformity has led to questions as to how spatial patterns of tree growth emerge over time. Spatially dependent growth of trees results from many factors; in particular, genotypic variation and microsite conditions are thought to greatly influence variation of tree structure within a plot (Schweingruber 1987, Downes et al. 2002). Variation in height-age trajectories amongst trees growing together in the same plot but of different genetic stocks is noted in the literature (Buford & Burkhart 1987, Magnussen & Kremer 1993, Tang et al. 2001). Both conceptually and mathematically, if non-clonal trees are planted together, there will always exist a confounding of genetic and microsite effects on tree growth (Buford & Burkhart 1987). A logical first step in understanding the underlying causes of spatially dependent tree growth is to understand how spatial patterns emerge in plots and to quantify those effects.

Simulations based on model forests are used by scientists to gain greater insights into a host of forestry issues (Tokolo & Shrestha 1999, Tomppo 2006, Hou et al. 2015). A large number of publications utilize simulations to better understand treatment outcomes, economic feasibility, and carbon sequestration with respect to climate change (Betts et al. 1997, Galbraith et al. 2010, Haynes et al. 1994, Huntingford et al. 2013, Prentice 1993, Scheller & Mladenoff 2005, Solomon 1986, Webster et al. 2003). Furthermore, simulations have been used by environmental scientists to better understand, compare, and verify statistical methods to be applied in the field (i.e. Borcard & Legendre 2002, Legendre et al.

2011, Peres-Neto et al. 2006, Peres-Neto & Legendre 2010, Hou et al. 2015). Simulations provide insight into future scenarios so that uncertainty can be minimized and management can adapt. One can use simulations to control environmental and spatial factors so that statistical methods can be applied in field-like conditions with the benefit of knowing actual plot conditions.

Induced spatial dependency can be produced by functional dependence of the response variables on explanatory variables that are themselves spatially correlated (Borcard & Legendre 2002). In our study, the response variables are the height and diameter of each tree and the explanatory variable is the site index (SI) - a measure of site productivity. We simulated plots with imbedded patterns of microsite productivity, thereby creating a functional dependence of height and diameter on the explanatory variables that are themselves spatially correlated. In our study, it is assumed that Y (height and diameter) has acquired the spatial structure of X (site index). If all important spatially-structured explanatory variables are included in the analysis, equation (1) correctly accounts for the spatial structure induced in Y .

$$y_j = f(X_j) + \varepsilon_j . \quad (1)$$

In equation (1), y_j is the value of the dependent variable y at site j and ε_j is the error term whose value is independent from tree to tree (Dray et al. 2012, Dale & Fortin 2014). If induced spatial dependency is occurring, then it should be properly accounted for in the model in order to perform correct standard statistical tests of the relationship between Y and X .

Testing of spatial effects requires that the spatial structure be expressed by meaningful spatial variables. The most straightforward method for modeling spatial relationships is polynomial regression where the geographic coordinates are used to generate trend surfaces (Legendre 1990, Borcard & Legendre 2002). However, trend surface is only satisfactory when the sampling area is approximately homogenous, the sampling design is closely regular, the number of spatial locations is “reasonable” (Norcliffe 1969), and the spatial structure to be modeled is somewhat simple (Dray et al. 2006). A more modern method of creating meaningful spatial variables is Moran’s eigenvector maps (MEM’s) (Dray et al. 2006). Moran eigenvector maps rely on eigenvector decomposition of truncated geographic distance matrix (Griffith & Peres-Neto 2006).

Our goal in this study is to reproduce the induced spatial dependence caused by microsite variability and measure the efficacy of redundancy analysis to test and quantify spatial effects. To meet this goal we analyze plots with a range of spatial pattern complexity and growth potential.

2. Methods

2.1 Study material and simulated data

This study simulated 5 hypothetical plots, each with a unique microsite design (Figure 1). The simulation produced tree height and diameter measurements similar to loblolly pine (*Pinus taeda L.*). Each plot consists of 25 rows and 25 columns of simulated trees. Trees are “planted” on 10-foot square spacing on ~1.43 acre plots. Each plot was assigned 1 of 5 microsite patterns. Microsite arrangements are distinct formations of high or low areas of productivity within each plot.

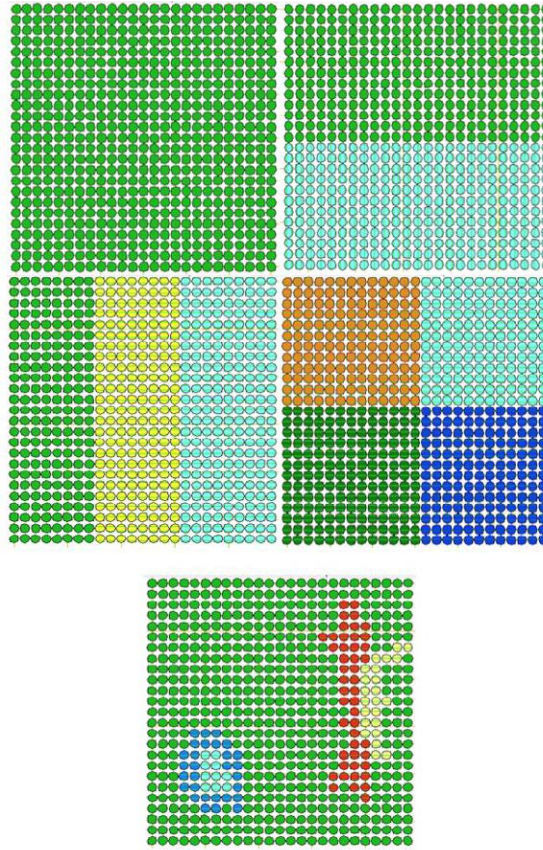


Figure 1. Illustration of the 5 spatial patterns used in this study. Microsites are distinguished by color. From left to right: Control, biplot, triplet, quadplot, and freeplot.

Plots were developed to represent a range of possible microsite patterns and most importantly, to induce spatial dependence by creating areas within a plot that have varying levels of productivity. By creating areas of high and low productivity, the size of each tree is dependent on its location in space. There are 1 to 5 microsites per plot represented by:

(Refer to Figure 1)

Control- The control plot has a single site index value because of microsite homogeneity. The SI value is 70 feet average dominant height at base age 25.

Biplot- Two microsites on the biplot, 70 feet average dominant height at base age 25 (green) and 80 feet average dominant height at base age 25 (blue).

Triplot- Three microsites of the triplot have a SI value of 60 feet average dominant height at base age 25 (yellow), 70 average dominant height feet at base age 25 (green), or 80 feet average dominant height at base age 25 (blue).

Quadplot- The quadplot has four microsites with SI value of 50 feet average dominant height at base age 25 (orange), 60 feet average dominant height at base age 25 (yellow), 70 feet average dominant height at base age 25 (green), or 80 feet average dominant height at base age 25 (blue).

Free plot- The free plot has five microsites. The large green area of the free plot is SI 70 feet average dominant height at base age 25. The small light blue area is SI 60 feet average dominant height at base age 25, the dark blue area circumscribing the blue area is SI 65 average dominant height feet at base age 25. The red area is SI 75 feet average dominant

height at base age 25 and the yellow area is SI 80 feet average dominant height at base age 25.

All calculations and simulations were done using R software. Since SI values are averages, we drew SI values for each individual tree from an assumed distribution. Assuming normality we state: $SI_{ijk} \sim N(\mu_j, \sigma_j^2)$ where the i th simulation ranges from $i=1 \dots S$, the j th microsite ranges from $j=1 \dots k$, and the k th tree ranges from $k=1 \dots K$. For estimating SI values we hold this condition true for each microsite: $CV_j = 0.10 = (\sigma_j \div \mu_j) * (100\%)$ where μ_j is the mean and CV_j is the coefficient of variation. We then used SI as our environmental variable $X_{ijk} = [SI_{ijk}]$. For the trees to reflect the spatial dependence (size of tree dependent on its location in space) caused by SI fluctuations within plots, we imposed different mean diameter at breast height (DBH) values for each microsite.

For k microsities we have $\mu_1 < \mu_2 < \dots < \mu_K$, where μ_K is the mean DBH for the K th microsite. For each simulation the CV was equal among all microsities. That is, $DBH_{ijk} \sim N(\mu_j, \sigma^2)$, where σ^2 is chosen to achieve a prespecified value of $CV = (\sigma \div \mu) * (100\%)$. Table 1 displays all 15 possible combinations examined for each spatial pattern. It should be noted, however, that the control plot only has 5 possible combinations (5 levels of CV 5%-25% and 0 levels of size difference) because there are no differences in mean DBH specified. As an example of treatment application, we can look at the biplot. In Table 1, the cell where CV=10% and difference in mean DBH=1 in. intersect, represents 1 of the 15 scenarios to be used in simulations for the biplot. In this example, the green portion of the biplot (see Figure 2) will contain trees with DBH values drawn from a normal distribution, $N(5, 0.25)$, and the blue portion will contain trees with DBH values drawn from the distribution $N(6, 0.36)$. These two distributions reflect the difference in mean DBH=1 in between the two microsities and variance calculations based on a 10% CV.

Table 1. Illustration of 15 possible scenarios for each spatial pattern with $k > 1$ microsities. Each scenario will be simulated for each spatial pattern. The control plot will be simulated with all 5 levels of CV.

		Coefficient of Variation				
		5%	10%	15%	20%	25%
Difference in mean DBH (inches)	0.5	(0.5,5%)	(0.5,10%)	(0.5,15%)	(0.5,20%)	(1,25%)
	1	(1,5%)	(1,10%)	(1,15%)	(1,20%)	(1,25%)
	2	(2,5%)	(2,10%)	(2,15%)	(2,20%)	(2,25%)

From DBH values we can then estimate total tree heights, which are calculated based on established diameter-height relationships. Equation (2) from Sabatia and Burkhart (2013) was used to model heights:

$$H_{ijk} = \frac{\beta_0 e^{\beta_1 DBH_{ijk}^{-1}}}{3.28} + \theta_{ijk} . \tag{2}$$

The parameter estimates from Sabatia and Burkhart (2013) are from a loblolly pine study of similar planting density. Where H_{ijk} is the total height (feet) and DBH_{ijk} is the diameter at breast height (inches) of the k th tree in the j th microsite of the i th simulation. The index

values range from, $i=1\dots S$, $j=1\dots k$, and $k=1\dots K$. For equation (2), β_0 is the upper asymptote parameter, β_1 is the rate parameter, and θ_{ijk} is the random error due to the k th tree [$\theta_{ijk} \sim N(0, \sigma_\theta^2)$] (Sabatia & Burkhart 2013). The estimated equation from Sabatia and Burkhart (2013) is then:

$$H_{ijk} = \frac{20.382e^{-7.309DBH_{ijk}^{-1}}}{3.28} + \theta_{ijk}, \theta_{ijk} \sim N(0, 0.5186). \quad (3)$$

We now have our response matrix $Y_{ijk}=[DBH_{ijk}, H_{ijk}]$. The last data we compute are the spatial variables. We simulated trees on a 10ft by 10ft planting grid and collected spatial information based on the Cartesian coordinate system. The tree in the top left position of the plot (origin position) has spatial coordinates (0,0), the tree to the immediate right of the origin has coordinates (10,0), the tree immediately beneath the origin has coordinates (0,10), and the tree down one row and to the right one column has coordinates (10,10). A pairwise matrix of distances (D_{qr}) was then constructed. D_{qr} contains the distances between each tree. A threshold value is chosen to truncate matrix D_{qr} . We used R software package PCNM (Legendre et al. 2012) for this analysis with default options that use the longest edge of the minimum spanning tree (Legendre et al. 2012), which in our case is 10ft. The following rule is then used to truncate D_{qr} :

$$D_{\text{trunc}(qr)} \begin{cases} D_{\text{trunc}(qr)} = D_{qr}, & \text{if } D_{qr} \leq \text{threshold} \\ D_{\text{trunc}(qr)} = 4 \times \text{threshold} & \text{if } i = j \\ D_{\text{trunc}(qr)} = 4 \times \text{threshold} & \text{if } D_{qr} \geq \text{threshold} \end{cases}$$

Next, a principal coordinate analysis (PCoA) was performed on $D_{\text{trunc}(qr)}$. The resulting principal coordinates are spatial eigenfunctions that model multiscale distance relationships among trees within each plot (Dray et al. 2006). We retained only the eigenvectors with positive eigenvalues (spatial variables) because they model positive spatial autocorrelation. Lastly, a forward selection of the remaining spatial variables is done to select significant spatial variables which compose the matrix W .

It should be noted that each iteration of the simulation process examines a “new” plot. For example, the biplot was simulated thousands of times throughout this study. Each iteration of the biplot holds only microsite pattern and spatial location of trees constant, but the trees take on different values for every simulation.

2.2 Redundancy Analysis

Redundancy analysis (RDA) (Rao 1964) is a method that extends multiple linear regression to multivariate linear regression involving multiple response variables and a common matrix on predictors. Variation partitioning for RDA with multivariate response and two sets of predictor matrices (X for environmental factors and W for spatial) are straightforward and applications for more than two predictor matrices are possible (Peres-Neto & Legendre 2010). Methods such as RDA utilize the spatial variables created with MEM's to estimate the contribution of spatial variation in the response data and filter out the effects of spatial correlation when testing the importance of ecological factors (Peres-Neto & Legendre 2010).

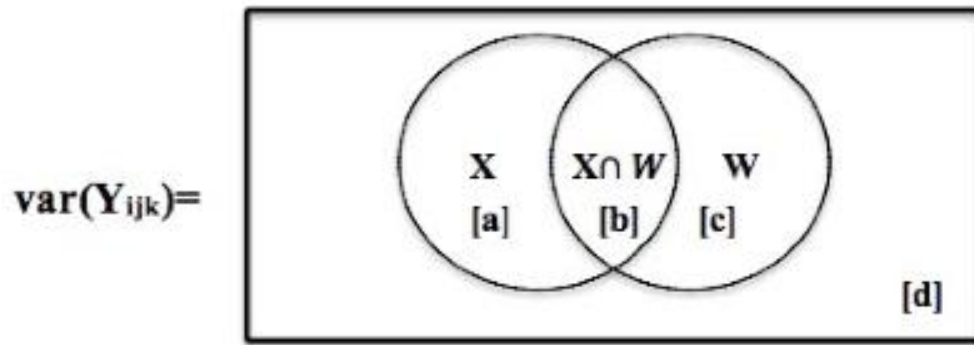


Figure 1. Illustration of the variation partitioning by RDA. Here, X and W are two explanatory matrices and [a], [b], [c], and [d] are fractions of variance. If matrix X is a matrix of environmental variables and W is a matrix of spatial variables then the fraction [a] is pure environmental variability, [b] is confounded variability of environmental and spatial, [c] is pure spatial, and [d] is the residual component. Fractions [a] and [c] are considered testable fractions and significance tests can be carried out by pRDA.

In this study, RDA was done using R software's "VEGAN" package (Oksanen et al. 2013). The first step to RDA is to standardize the response variables (Borcard et al. 1992). The response variables mentioned hereafter are considered standardized. This symmetric form of analysis utilizes a response matrix $Y_{625 \times 2}$ (hereafter Y), where $625=25$ rows \times 25 columns, and with explanatory vector $X_{625 \times 1}$ (hereafter X) and covariables $W_{625 \times 2}$ (hereafter W). In RDA, the ordination axes are obtained by a PCA of \hat{Y} , which is computed by fitting the Y variables to X by multivariate linear regression (Laliberté et al. 2009). An important characteristic of the RDA process is that the ordination of Y produces ordination axes that are linear combinations of X (Peres-Neto & Legendre 2010, ter Braak & Prentice 1988). Multiple linear regression on all variables in X is done for each variable in Y and $\hat{\beta} = [X^t X]^{-1} X^t Y$ is calculated (Peres-Neto et al. 2006).

The canonical R^2 , called the bivariate redundancy statistic by Miller & Farr (1971), quantifies the strength of the linear relationship between variables Y and X, where \hat{Y} are the multivariate estimated values of the response:

$$R_{Y|X}^2 = \frac{SS(\hat{Y})}{SS(Y)}. \quad (4)$$

In equation (4), $SS(\hat{Y})$ is the total sum of squares of \hat{Y} and $SS(Y)$ is the total sum of squares of Y. We construct an equivalent adjusted R^2 measure to the one introduced by Ezekiel (1930), denoted by rR^2 , where n is the number of observations and m is the number of degrees of freedom in the fitted model:

$$rR^2 = 1 - (1 - R_{Y|X}^2) \frac{n-1}{(n-m-1)}. \quad (5)$$

Referring to Figure 2, we can begin to calculate the fractional explained variance components (a,b, and c) as well as the unexplained variance component (d) by following steps outlined by Legendre (2008). Variation partitioning of Y results from three simple RDA's each with a different independent matrix. For example, we used X, W, and X|W to

estimate variation from environmental, spatial, and environmental and spatial variables, respectively.

We followed this procedure for each iteration of our simulation. Referring to Table 1, there are 5 scenarios for the control plot (only changes in CV can be used since there are no microsites) and 15 combinations of CV and difference in mean DBH for the biplot, triplot, quadplot, and free plots. For each of these scenarios 1000 simulations were run and the rR^2 values were collected. After the 1000 simulation runs an estimate of pure spatial variation is obtained for given spatial patterns and scenarios.

2.3 Partial Redundancy Analysis

Partial RDA can test an individual explanatory matrix while controlling for the linear effects of a second matrix containing covariables (Legendre et al 2011). In pRDA we are able to isolate and test for pure effects (ter Braak & Smilauer 2002). The most compelling function of pRDA is that one can test for pure effects of spatial, environmental, chemical, treatment, and other components while controlling for the linear effects of other covariables (Legendre et al 2011).

Partial redundancy analysis was conducted using R software's "VEGAN" package (Oksanen et al. 2013). Matrices X and W are interchangeable, depending on which partial variance is to be tested. For our specific objectives, we tracked the significance testing of $Y \sim W|X$. This is the hypothesis of spatial dependence and tests the significance of fraction [c], (see Figure 2) representing pure spatial variation. A two-stage approach to testing the significance of the pure spatial component was taken. First, the software calculated the R^2 statistic of partial regression:

$$R_{Y \sim W|X}^2 = \frac{SS(Y \sim W|X)}{SS(Y \sim W)} \quad (6)$$

Following this calculation, the F-statistic was used to test the overall significance of the partial regression relationship is:

$$F = \frac{R_{Y \sim W|X}^2}{m} \cdot \frac{1 - R_{Y \sim W|X}^2}{n - 1 - m - q} \quad (7)$$

Where n is the number of observations, m is the number of parameters, and q is the number of covariables in W. Significance of the F -statistic may be tested with the F -distribution if the assumption of normality of the residuals holds and the data are standardized. However this is rarely the case in many ecological studies, and for this reason, permutation tests are preferred and are used in this study. Specifically, we used a permutation of the residuals of the reduced model.

The null hypothesis for the partial F -test of $X|W$ states that the response is not spatially dependent. For each of the spatial patterns all applicable scenarios in Table 1 were simulated 1000 times, and for each iteration of the simulation a permutation F -test was performed (999 permutations per test). Each iteration of the simulation was considered a Bernoulli trial and assigned a 1, if the null hypothesis was rejected, and 0 otherwise. After simulations, the efficacy of pRDA in detecting spatial dependency was estimated by calculating the probability of success as the average of all trials.

3. Results

3.1 Redundancy Analysis

We used RDA to perform a variation partitioning to estimate the pure spatial variability. Table 2 contains the estimated rR^2 value associated with the pure spatial component. As discussed earlier, there are 15 scenarios per spatial pattern. The scenarios are a combination of differences in mean DBH and CV as shown in Table 1. Notably, the rR^2 values for the control plot are 12-13%. The largest rR^2 values are usually in the quadplot, which is one of the more complex patterns. More variation tends to be captured in scenarios with larger differences in DBH and lower values of CV. The amount of variation explained tends to increase from control plot to triplot or quadplot before decreasing.

Table 2 Estimated rR^2 for each spatial pattern and all scenarios.

Coefficient of Variation	Control	Biplot	Triplot	Quadplot	Free	
5%	13%	6%	46%	24%	24%	0.5 inch
10%	13%	10%	29%	19%	20%	
15%	13%	11%	22%	16%	16%	
20%	13%	12%	18%	15%	15%	
25%	12%	13%	16%	14%	13%	
Coefficient of Variation	Control	Biplot	Triplot	Quadplot	Free	
5%	13%	3%	62%	76%	22%	1 inch
10%	13%	7%	52%	67%	20%	
15%	13%	9%	41%	55%	18%	
20%	13%	10%	33%	44%	16%	
25%	12%	12%	27%	36%	15%	
Coefficient of Variation	Control	Biplot	Triplot	Quadplot	Free	
5%	13%	0%	68%	76%	20%	2 inch
10%	13%	3%	63%	72%	19%	
15%	13%	5%	55%	66%	19%	
20%	13%	7%	47%	59%	18%	
25%	12%	8%	40%	50%	17%	

3.2 Partial Redundancy Analysis

Partial redundancy analysis was used to detect spatial dependence. The results reported are the probability of detecting spatial dependence for all combinations of spatial patterns and scenarios. Table 3 contains the results from the pRDA simulations.

Table 3 Illustration of the results from pRDA. The values represent the probability of detecting spatial dependence.

Coefficient of Variation	Control	Biplot	Triplot	Quadplot	Free	
5%	0.04	1	1	0.99	1	0.5 inch
10%	0.06	0.88	0.86	0.99	1	
15%	0.04	0.77	0.51	0.9	1	
20%	0.06	0.58	0.39	0.8	1	
25%	0.04	0.51	0.31	0.8	1	
Coefficient of Variation	Control	Biplot	Triplot	Quadplot	Free	
5%	0.04	1	1	1	1	1 inch
10%	0.06	1	0.98	0.99	1	
15%	0.04	0.96	0.92	0.98	1	
20%	0.06	0.93	0.85	0.86	1	
25%	0.04	0.86	0.56	0.77	1	
Coefficient of Variation	Control	Biplot	Triplot	Quadplot	Free	
5%	0.04	1	1	1	1	2 inch
10%	0.06	1	1	1	1	
15%	0.04	1	1	1	1	
20%	0.06	0.99	0.97	0.98	1	
25%	0.04	1	0.83	0.92	1	

The highest probabilities for detection are for the free plot and with larger differences in DBH among microsites. The probability for detecting spatial dependence in the control plot is consistently at approximately 0.05. This reflects the type 1 error rate of $\alpha = 0.05$, which is the probability of rejecting the null hypothesis when the null hypothesis is true.

4. Discussion

4.1 Redundancy Analysis

The variation partitioning and quantification of spatial variability performed as expected. Referring to Table 2, we see there is no distinct pattern in the amount of spatial variation captured. This confirms that spatial pattern complexity and perhaps the shape of microsites can influence the efficacy of RDA to capture spatial variability. Even if there are no obvious patterns in how rR^2 changes with spatial pattern complexity, one can still see that large differences among spatial pattern reflected in rR^2 . It is possible that the spatial processes, in the biplots, for example, show fortuitous correlations with the environmental variable (Bell et al. 2006). The rR^2 of the control plots ranges from 12-13%. This observed spatial variation is simulated by chance, but it happens to reflect realistic measures of variability in a seemingly random or aggregated tree growth. Lepš and Kindlmann (1987) noted in their study that it is incorrect to deduce the independence of individuals within a

population from an observed random pattern. The results from this portion of the simulation study were very promising. The values from Table 2 are rR^2 values, and we expected them to be rather low (<10%), but found values as high as 76%. The largest portions of variation explained by the spatial component were found in the scenarios with the greatest difference in mean DBH and in more complex spatial patterns.

The difference in mean DBH among microsites was examined at three levels (0.5in, 1in, 2in). As the difference in mean DBH increases among microsites, the rR^2 values increase as well. This trend is intuitive. By implementing larger differences in mean DBH we are essentially creating stronger and more obvious spatial dependencies. Redundancy analysis is detecting the stronger relationship between size and spatial location. Coefficient of variation is very influential in how much spatial variability is captured.

In Table 2, as expected, CV increase the rR^2 decreases. The amount of variation used to draw DBH values for each microsite blurs the line, so to speak, between microsites. Graphing the DBH distributions of each microsite simultaneously shows increased overlap of the distributions with increased values of CV. Conceptually, as overlap among the distributions increases, there is an increase towards uniformity and thus spatial dependencies become less obvious.

4.2 Partial Redundancy Analysis

We used pRDA simulations to measure the probability of successfully detecting spatial dependency with permutation F -tests which looked at the significance of the “pure spatial” component. These results are promising, with many scenarios showing greater than .80 probability of success and some with a success probability of 1. These results are promising because we observed higher success rates in the most complex spatial pattern, which contained smaller more frequent microsites. This may be the most realistic spatial pattern. Palmer (1980), who quantified spatial patterns of plant environment relationships in hardwood plots, found that most of the spatial dependence measured in his variables were at small scales (within 10 meter subplots). Our results indicate that spatial patterns with smaller, more frequent microsites more often had significant spatial variables. The trends observed are surprising. An increase in spatial pattern complexity increases the probability of successful detection. More influential than pattern complexity is difference in mean DBH.

As difference in mean DBH increases, the probability of detecting spatial dependency increases. The increase in mean difference in DBH creates more obvious spatial dependencies and less overlap among distributions of microsites. The largest effect seems to result from increases in CV.

As CV increases, the probability of detecting spatial dependency decreases. The increased amount of variation in each microsite actually increases the uniformity of the plot and assuages the effects of spatial dependencies. Therefore, it becomes increasingly more difficult to detect spatial dependency with higher amounts of variation.

The probability of detecting spatial dependence of the control plot for all scenarios was approximately 0.05. This is a reassuring statistic because it validates the statistical methods used. An $\alpha=0.05$ for the permutation F -tests was specified before running the simulations. Therefore, about 5% of the time we would expect the test to detect spatial dependence when there is none.

References

- Bell, G., Lechowicz, M. J., & Waterway, M. J. (2006). The comparative evidence relating to functional and neutral interpretations of biological communities. *Ecology*, *87*(6), 1378-1386.
- Betts, R. A., Cox, P. M., Lee, S. E., & Woodward, F. I. (1997). Contrasting physiological and structural vegetation feedbacks in climate change simulations. *Nature*, *387*(6635), 796-799.
- Borcard, D. & Legendre, P. (2002). All-scale spatial analysis of ecological data by means of principal coordinates of neighbour matrices. *Ecological Modelling*, *153*(1), 51-68.
- Buford, M. A. & Burkhart, H. E. (1987). Genetic improvement effects on growth and yield of loblolly pine plantations. *Forest Science*, *33*(3), 707-724.
- Dray, S., Legendre, P., & Peres-Neto, P. R. (2006). Spatial modelling: a comprehensive framework for principal coordinate analysis of neighbour matrices (PCNM). *Ecological Modelling*, *196*(3), 483-493.
- Dray, S., Pélissier, R., Couteron, P., Fortin, M. J., Legendre, P., Peres-Neto, P. R., & Wagner, H. H. (2012). Community ecology in the age of multivariate multiscale spatial analysis. *Ecological Monographs*, *82*(3), 257-275.
- Dale, M. R. & Fortin, M. J. (2014). *Spatial analysis: a guide for ecologists*. Cambridge University Press.
- Downes, G. M., Wimmer, R., & Evans, R. (2002). Understanding wood formation: gains to commercial forestry through tree-ring research. *Dendrochronologia*, *20*(1), 37-51.
- Dray, S., Legendre, P., & Peres-Neto, P. R. (2006). Spatial modelling: a comprehensive framework for principal coordinate analysis of neighbour matrices (PCNM). *Ecological Modelling*, *196*(3), 483-493.
- Ezekiel, M. (1930). *Methods of correlation analysis*. 427 pp., illus. *New York and London*. Chicago
- Fox, J. C., Ades, P. K., & Bi, H. (2001). Stochastic structure and individual-tree growth models. *Forest Ecology and Management*, *154*(1), 261-276.
- Galbraith, D., Levy, P. E., Sitch, S., Huntingford, C., Cox, P., Williams, M., & Meir, P. (2010). Multiple mechanisms of Amazonian forest biomass losses in three dynamic global vegetation models under climate change. *New Phytologist*, *187*(3), 647-665.
- Griffith, D. A. & Peres-Neto, P. R. (2006). Spatial modeling in ecology: the flexibility of eigenfunction spatial analyses. *Ecology*, *87*(10), 2603-2613.
- Haynes, R. W., Alig, R. J., & Moore, E. (1994). Alternative simulations of forestry scenarios involving carbon sequestration options: Investigation of impacts on regional and national timber markets. Forest Service general technical report (No. PB-95-128856/XAB; FSGTR-PNW--335). Forest Service, Portland, OR (United States). Pacific Northwest Research Station.
- Hou, Z., Xu, Q., Hartikainen, S., Antilla, P., Packalen, T., Maltamo, M., & Tokola, T. (2015). Impact of Plot Size and Spatial Pattern of Forest Attributes on Sampling Efficacy. *Forest Science*, *61*(5), 847-860.
- Huntingford, C., Zelazowski, P., Galbraith, D., Mercado, L. M., Sitch, S., Fisher, R., & Cox, P. M. (2013). Simulated resilience of tropical rainforests to CO₂-induced climate change. *Nature Geoscience*, *6*(4), 268-273.
- Laliberté, E., Paquette, A., Legendre, P., & Bouchard, A. (2009). Assessing the scale-specific importance of niches and other spatial processes on beta diversity: a case study from a temperate forest. *Oecologia*, *159*(2), 377-388.

- Legendre, P. (1990). Quantitative methods and biogeographic analysis. In *Evolutionary Biogeography of the Marine Algae of the North Atlantic* (pp. 9-34). Springer Berlin Heidelberg.
- Legendre, P., Oksanen, J., & ter Braak, C. J. (2011). Testing the significance of canonical axes in redundancy analysis. *Methods in Ecology and Evolution*, 2(3), 269-277.
- Legendre, P. (2011). const. clust: space-and time-constrained clustering package. R package version 1.2. URL: <http://adn.biol.umontreal.ca/~numericalecology/Rcode>.
- Legendre, P., Borcard, D., Blanchet, F. G., & Dray, S. (2012). PCNM: MEM spatial eigenfunction and principal coordinate analyses. R package version 2.1-2/r106.
- Legendre, P. & Legendre, L. F. (2012). *Numerical ecology* (Vol. 24). Elsevier.
- Lepš, J. & Kindlmann, P. (1987). Models of the development of spatial pattern of an even-aged plant population over time. *Ecological Modelling*, 39(1), 45-57.
- Magnussen, S. & Kremer, A. (1993). Selection for an optimum tree growth curve. *Silvae Genetica*, 42(6), 322-322.
- Marignani, M., Del Vico, E., & Maccherini, S. (2007). Spatial scale and sampling size affect the concordance between remotely sensed information and plant community discrimination in restoration monitoring. *Biodiversity and Conservation*, 16(13), 3851-3861.
- Mateu, J., Uso, J. L., & Montes, F. (1998). The spatial pattern of a forest ecosystem. *Ecological Modelling*, 108(1), 163-174.
- Miller, J. K., & Farr, S. D. (1971). Bimultivariate redundancy: a comprehensive measure of interbattery relationship. *Multivariate Behavioral Research*, 6(3), 313-324.
- Norcliffe, G. B. (1969). On the use and limitations of trend surface models. *The Canadian Geographer/Le Géographe Canadien*, 13(4), 338-348.
- Oksanen, J., Blanchet, G., Kindt, R., Legendre, P., Minchin, P.R., O'Hara, R.B., Simpson, G., Solymos, P., Stevens, M., and Wagner, H. (2013). "Package 'vegan'." *R Packag ver* 254: 20-8.
- Palmer, M. W. (1990). Spatial scale and patterns of species-environment relationships in hardwood forest of the North Carolina Piedmont. *Coenoses*, 5(2), 79-87.
- Penttinen, A., Stoyan, D., & Henttonen, H. M. (1992). Marked point processes in forest statistics. *Forest Science*, 38(4), 806-824
- Peres-Neto, P. R., Legendre, P., Dray, S., & Borcard, D. (2006). Variation partitioning of species data matrices: estimation and comparison of fractions. *Ecology*, 87(10), 2614-2625.
- Peres-Neto, P. R. & Legendre, P. (2010). Estimating and controlling for spatial structure in the study of ecological communities. *Global Ecology and Biogeography*, 19(2), 174-184.
- Prentice, I. C., Sykes, M. T., & Cramer, W. (1993). A simulation model for the transient effects of climate change on forest landscapes. *Ecological Modelling*, 65(1), 51-70.
- Rao, C. R. (1964). The use and interpretation of principal component analysis in applied research. *Sankhyā: The Indian Journal of Statistics, Series A*, 26(4), 329-358.
- Sabatia, C. O. & Burkhart, H. E. (2013). Height and diameter relationships and distributions in loblolly pine stands of enhanced genetic material. *Forest Science*, 59(3), 278-289.
- Scheller, R. M. & Mladenoff, D. J. (2005). A spatially interactive simulation of climate change, harvesting, wind, and tree species migration and projected changes to forest composition and biomass in northern Wisconsin, USA. *Global Change Biology*, 11(2), 307-321.
- Schweingruber, F.H. (1987). *Tree Rings: Basics and Applications of Dendrochronology*. Kluwer Academic Publishers, Dordrecht.

- Solomon, A. M. (1986). Transient response of forests to CO₂-induced climate change: simulation modeling experiments in eastern North America. *Oecologia*, 68(4), 567-579.
- Tang, S., Meng, F. R., & Bourque, C. P. A. (2001). Analyzing parameters of growth and yield models for Chinese fir provenances with a linear mixed model approach. *Silvae Genetica*, 50(3-4), 140-145.
- ter Braak, C. J. & Prentice, I. C. (1988). A theory of gradient analysis. *Advances in Ecological Research*, 18, 271-317.
- ter Braak, C. J., & Smilauer, P. (2002). *CANOCO reference manual and CanoDraw for Windows user's guide: software for canonical community ordination (version 4.5)*. www.canoco.com.
- Tokola, T. & Shrestha, S. M. (1999). Comparison of cluster-sampling techniques for forest inventory in southern Nepal. *Forest Ecology and Management*, 116(1), 219-231.
- Tomppo, E. (2006). The Finnish national forest inventory. In *Forest Inventory* (pp. 179-194). Springer Netherlands.
- Webster, M., Forest, C., Reilly, J., Babiker, M., Kicklighter, D., Mayer, M., Prinn, R., Sarofim, M., Sokolov, A., Stone, P. & Wang, C. (2003). Uncertainty analysis of climate change and policy response. *Climatic Change*, 61(3), 295-320.